7-26-2022

The interaction of deep eutectic solvents with pristine carbon nanotubes and their associated defects: A density functional theory study

Hamid Reza Ghenaatian
Department of Physics, Jahrom University

Mehdi Shakourian-Fard
Department of Chemical Engineering, Birjand University of Technology,

Ganesh Kamath
Dalzierfiver LLC, 3500 Carlfied St, EL Sobrante, CA

John F. Trant
niversity of Windsor, Department of Chemistry and Biochemistry, 401 Sunset Ave., Windsor, Ontario

Farouq S. Mjalli
Department of Petroleum & Chemical Engineering, Sultan Qaboos University, Muscat. Oman

Ghenaatian, Hamid Reza, et al. “The Interaction of Deep Eutectic Solvents with Pristine Carbon Nanotubes and Their Associated Defects: A Density Functional Theory Study.” *Journal of Molecular Liquids*, vol. 363, Oct. 2022, p. 119855. *DOI.org (Crossref)*, https://doi.org/10.1016/j.molliq.2022.119855.

The Interaction of Deep Eutectic Solvents with Pristine Carbon Nanotubes and Their Associated Defects: A Density Functional Theory Study

Hamid Reza Ghenaatian,[*a] Mehdi Shakourian-Fard,[b] Ganesh Kamath,[c] John F. Trant,[d] Farouq S. Mjalli[e]

[a] Department of Physics, Jahrom University, Jahrom, P.O. Box 74135-111, Iran.
[b] Department of Chemical Engineering, Birjand University of Technology, Birjand, P.O. Box 97175/569, Iran.
[c] Dalzierfiver LLC, 3500 Carlfied St, EL Sobrante, CA 94803, USA.
[d] University of Windsor, Department of Chemistry and Biochemistry, 401 Sunset Ave., Windsor, Ontario N9B 3P4, Canada.
[e] Department of Petroleum & Chemical Engineering, Sultan Qaboos University, Muscat. Oman

[*]Corresponding author:

E-mail: Ghenaat@jahromu.ac.ir

Abstract

In this study, the interaction of four deep eutectic solvents (DESs): [Choline chloride][Urea] ([ChCl][U]), [Choline chloride][Ethylene glycol] ([ChCl][EG]), [Choline chloride][Glycerol] ([ChCl][Gly]) and [Choline chloride][Benzoic acid] ([ChCl][BA]), with pristine carbon nanotube (CNT) and its defects: double-vacancy and Stone–Wales structures (CNT-DV and CNT-SW) is investigated using density functional theory (DFT) calculations. The geometry optimization, electronic property calculations, noncovalent interaction analysis and optical properties of the DES@nanotube complexes were carried out at the M06-2X/cc-pVDZ level of theory. The adsorption energy (E_{ads}) calculations show that the presence of the DV and SW defects on the CNT increases the adsorption strength of the DESs, DES@CNT-SW > DES@CNT-DV > DES@CNT. On the other hand, the adsorption energy values increase with an increase in the volume of DESs due to the increase of noncovalent interactions, following the order [ChCl][BA]> [ChCl][Gly]> [ChCl][U]> [ChCl][EG]. The calculation of the HOMO-LUMO energy gap (E_g) and chemical hardness (η) of the DES@nanotube complexes indicates that the DES@CNT-SW complexes have the largest E_g and η values and thus the lowest chemical reactivity. The analysis of the interactions

between the nanotubes and the DESs using noncovalent interaction (NCI) plots and energy decomposition analysis (EDA) suggests that the DESs adsorb onto the nanotubes through van der Waals interactions and that dispersive interactions dominate (dispersion interaction energy (ΔE_{disp}) > electrostatic interaction energy (ΔE_{elec}) > orbital interaction energy (ΔE_{orb})). Predicted ultraviolet–visible absorption spectra of the complexes show that the adsorption of DESs on the nanotubes has only a very marginal effect on the optical response of the nanotubes. Transition density matrix heat maps reveal that the electrons and holes localize to the CNT, CNT-DV and CNT-SW surfaces in the DES@nanotube complexes, indicating that the charge transfer occurs mostly on the surfaces.

Keywords: Carbon nanotube (CNT), Stone-Wales defects, Double-vacancy defects, Deep eutectic solvents, Noncovalent interaction, DFT

1. Introduction

Over the last few decades, deep eutectic solvents (DESs) are being increasingly considered as a viable alternative to traditional volatile solvents due to their easy recyclability, effective thermal stability, and consequent cost effectiveness [1, 2]. DESs, first reported by Abbott in 2001 [3], are prepared by combining two or more immiscible solid components at appropriate molar ratios, which upon mixing liquify with a freezing point lower that any individual component. They are related to ionic liquids (ILs) but don't require the preformation of a salt, and may or may not be ionic. DESs are often biodegradable, show lower toxicity than ILs, and normally require no synthesis other than physically mixing inexpensive industrial chemicals [4-6]. Generally, DESs employ the counterions of quaternary ammonium or phosphonium cations as a hydrogen-bond acceptor (HBA) and amides, carboxylic acids, or polyols as a hydrogen-bond donor (HBD) [7, 8]. This generates a mixture where the hydrogen bond network interrupts the poorly coordinating ionic species creating an amorphous and dynamic milieu. The strength of the emergent electrostatic, hydrogen bonding and dispersion interactions determines the properties of the DESs.

Nanostructured materials with extremely high surface areas have opened a new rich world of possibilities in science and industry [9, 10]. The first reported application of DESs in nanotechnology was in 2008 for the synthesis of gold nanoparticles [11]. Since then, DESs have been employed to tune the synthesis and functionality of nanoscale materials [12, 13]; the

combinatorial nature of DES, where the properties can be easily adjusted by simply mixing different components, makes them promising solvents for fine tuning of the desired properties in the nanoscale materials.

Carbon nanotubes (CNTs) are promising nanostructure materials with high porosity, low density, and extreme tensile strength [14]. The hype around these materials for hydrogen storage or structural applications is significant, and although the full promise has not been fulfilled, they are beginning to show utility for a variety of applications. But one of the limitations is that the theory supposes perfect CNTs. Synthesis is rarely perfect, and most CNTs incorporate a series of defects such as vacancies, non-hexagonal rings (pentagons or heptagons) and dopants (both intended and contaminating). However, although these defects are undesirable for mechanical applications, weakening the ideal infinite periodic sp^2 hexagon cylindrical sheets, theoretical and experimental studies have both suggested that imperfections can lead to more interesting electrical and chemical behavior [15-18]. Other molecules can more easily interact with the surface where the perfection in the electronic balance is disturbed, creating dipoles and edges that can form stronger dispersion interactions.

Binding energy measurements can be used to estimate the effects of defects on the interaction of CNTs with other species. For example, Baldo and co-workers developed back-gated field effect transistors (FETs) made of carbon nanotubes for gas sensing applications. Their results for NH_3 and NO_2 sensing showed that the sensitivity to each gas depends on the kind of CNTs used for the device. They showed that the interaction strength of the structural or chemical defects in CNTs with NH_3 and NO_2 gas molecules affects the behavior of devices [19]. Nagih and colleagues introduced an ethylene sensing device based on defective CNTs at low temperatures and very low gas concentrations. They proposed that their good sensing performance was achieved due to the presence of structural defects in CNTs [20]. DESs can stabilize CNT solutions especially if they are used as functionalization agents [21, 22], as they show excellent affinity for the surface. However, only a few reports have studied the interaction of DESs with CNTs experimentally: Yan et al. investigated the stability of numerous nanofluids consisting of various DESs and CNTs in different concentrations through visual observation and UV spectroscopy [23], and Walvekar and coauthors studied the potential of DESs as base fluids to prepare CNT nanofluids [24].

Computational chemistry has now become routine for studying interactions at the atomic and molecular level, offering cost-effective, accurate, and time-saving screening tools to analyze and

predict the behavior of materials [25]. Nevertheless, only a few computational studies have effectively modeled the interactions of DESs with nanomaterials. For instance, Aparicio and co-workers studied the adsorption properties of choline chloride-based DESs on graphene and the behavior of the corresponding nanodroplets using density functional theory (DFT) and classical molecular dynamics (MD) simulations [26]. They also studied the properties of carbon, boron nitride, silicon, germanium, and molybdenum disulfide nanotubes in the DES reline ([choline chloride][urea]) using classical molecular dynamics simulations [27]. Recently, we applied DFT calculations to investigate the adsorption properties of DESs on the graphene surfaces and its defective double-vacancy and Stone–Wales forms [28] as well as boron-nitride surface and its defective forms containing boron and nitrogen vacancies [29]. However cylindrical surfaces could behave differently.

To the best of our knowledge, this is the first DFT study comprehensively investigating the adsorption of DESs on carbon nanotubes (CNTs) and their defective structures with the goal of understanding how defects affect behavior. This work is limited to the study of the adsorption of four of the more common DESs. All use choline chloride ([ChCl]) as the hydrogen bond acceptor (HBA), and use, in turn, urea ([U]) [30], ethylene glycol ([EG]) [31], glycerol ([Gly]) [32], or benzoic acid ([BA]) [33] as hydrogen bond donor (HBD). Among all the HBDs, the [BA] is the only molecule with a six-membered aromatic ring in its structure. The aim of the use of [BA] as HBD in this study is to understand the effect of the presence of aromatic ring in the HBD and π-π interactions on the adsorption strength of DESs on the CNTs and their defects.

In this study, the interaction of these four DESs with carbon nanotubes (CNTs) and CNTs containing two of the most important defects, including double-vacancy and Stone–Wales defects is investigated using the M06-2X functional and cc-pVDZ basis set. The nature and strength of interactions between the surfaces and DESs are considered using techniques such as atoms in molecules analysis, non-covalent interaction plots and energy decomposition analysis.

2. Computational details

There are two important types of common defects in the CNTs: double-vacancy (5-8-5) defects and Stone–Wales (55-77) defects. The double-vacancy (5-8-5) defect is formed by the removal of two carbons, leaving a surface with two pentagonal rings and one octagonal ring [34]. On the other hand, the Stone–Wales (55-77) defect is produced by the rearrangement of the six-

membered rings in the CNTs into two five (pentagons) and two seven (heptagons) rings. This rearrangement is a result of 90° rotation of a C–C bond [35]. The geometries of the pristine CNT ($C_{96}H_{16}$), CNT containing double vacancy (CNT-DV; $C_{94}H_{16}$) and Stone-Wales (CNT-SW; $C_{96}H_{16}$) defects, DESs and their complexes (DES@nanotube) were optimized using the M06-2X functional corrected by Grimme's D3 correction [36] with the cc-pVDZ basis set. This method and basis set have proven reliable for determining the structures, binding energies and the nature of noncovalent interactions responsible for adsorption of liquids and DESs on the graphene, hexagonal boron nitride and their defective forms [37-40], nitrogen-doped graphene [41] and fluorographene [42] surfaces. The DES are identical to those we analyzed in our previous work [28], and the calculations of the optimized geometries of these species were drawn from that effort and not-reperformed. The CNT, CNT-DV and CNT-SW models have an armchair (4,4) symmetry and a singlet ground state. In these models, the terminal carbon atoms are saturated with hydrogen atoms to avoid the boundary effects [43]. These models are sufficiently large to adequately model their interaction with the DESs at their midpoint. All quantum chemical calculations were performed using the Gaussian 09 D.01 suite of programs [44]. In order to ensure that the stationary points are real minimum points, the vibrational frequencies were calculated at the same level of theory. A limitation of the study is that it does focus on a single DES interacting with the surface. This is an acceptable simplification, but a refined accuracy will be obtained with far larger systems that will become computationally feasible at this required level of theory in the future.

The adsorption energy (E_{ads}) values for adsorption of DESs on the surfaces were calculated according to the following equation:

$$E_{ads} = E_{(DES@nanotube)} - [E_{(DES)} + E_{(nanotube)}] + E_{(BSSE)} \quad \text{(Equation 1)}$$

Nanotube: CNT, CNT-DV and CNT-SW

DES: [ChCl][U], [ChCl][EG], [ChCl][Gly], and [ChCl][BA]

In this equation, $E_{(DES@nanotube)}$ term is the energy of the adsorption complex, $E_{(DES)}$ term is the energy of the non-adsorbed DESs, $E_{(nanotube)}$ is the energy of the nanotubes. The $E_{(BSSE)}$ term represents the basis set superposition errors (*BSSEs*) to correct the adsorption energies. The *BSSE* values are calculated based on the Boys-Bernardi counterpoise method [45].

The atomic charge analysis on the optimized geometries was performed using the ChelpG method [46]. The magnitude of charge transfer in the DES@nanotube complexes was obtained

through the calculation of ChelpG charge [46] on the nanotube in the DES@nanotube complexes. In order to find the possible initial structures for interaction of DESs with the surfaces, the electrostatic potential (ESP) maps for the DESs and nanotubes were generated with the "cubegen" utility of the Gaussian 09 D.01 suite of programs [44]. Global molecular descriptors such as HOMO-LUMO energy gap ($E_g = E_{LUMO} - E_{HOMO}$) and chemical hardness ($\eta = E_{LUMO} - E_{HOMO}/2$) were calculated for the DES@nanotube complexes [47]. The molar van der Waals volume (V_m) of the DESs was calculated by using van der Waals radii for the atoms of DESs and molecular geometries yielded by the DFT calculations. In order to analyze the role of noncovalent interactions in the adsorption process, a detailed study was carried out using noncovalent interaction (NCI) plots [48] and an energy decomposition analysis (EDA) [49, 50]. The NCI plots were calculated using Multiwfn 3.7 program [51] and plotted using VMD 1.9.3 [52]. The EDA was carried out at the PBE-D3/TZP level of theory using the Amsterdam Density Functional (ADF) (2013.01) package [53-55]. The UV-visible absorption spectra of the CNT, CNT-DV, CNT-SW nanotubes, and their complexes with the DESs were considered for 10 excited states using the TD-M06-2X/cc-pVDZ level of theory. The excited-state properties and the fragment transition density matrix (FTDM) maps were calculated and plotted using Multiwfn 3.7 program [51].

3. Results and discussion

3.1. Structure of DESs

In our previous work on these DES with other surfaces, we had already identified the preferred geometries of the studied DES [28, 29]. Briefly, in order to find a stable geometry for the DESs, the interaction sites of the DES components including $[Cl]^-$ anion, $[Ch]^+$ cation, [ChCl] salt as a hydrogen bond acceptor (HBA), and hydrogen bond donors (HBDs) of [U], [EG], [Gly], and [BA] were considered by calculating their electrostatic potential (ESP) maps (Figure S1).

As seen from Figure S1, the negative and positive electrostatic potentials are primarily localized to the $[Cl]^-$ anion and $[Ch]^+$ cation, respectively. According to the ESP maps of the $[Cl]^-$ anion and $[Ch]^+$ cation, the possible initial structures for the interaction of $[Cl]^-$ anion with $[Ch]^+$ cation were determined by initially placing the $[Cl]^-$ anion (with negative electrostatic potential) close to the regions with positive electrostatic potential on the $[Ch]^+$ cation at a distance of 2.7 Å. Subsequently, these structures were optimized at the M06-2X/cc-pVDZ level of theory and sorted

according to their energy. The optimized structure with the lowest energy was identified as the most stable geometry of the [ChCl] salt and is shown in Figure 1. This work was not reperformed for this study, and further details of these specific calculations can be found in our previous publications looking at these DESs for other surfaces [28, 29].

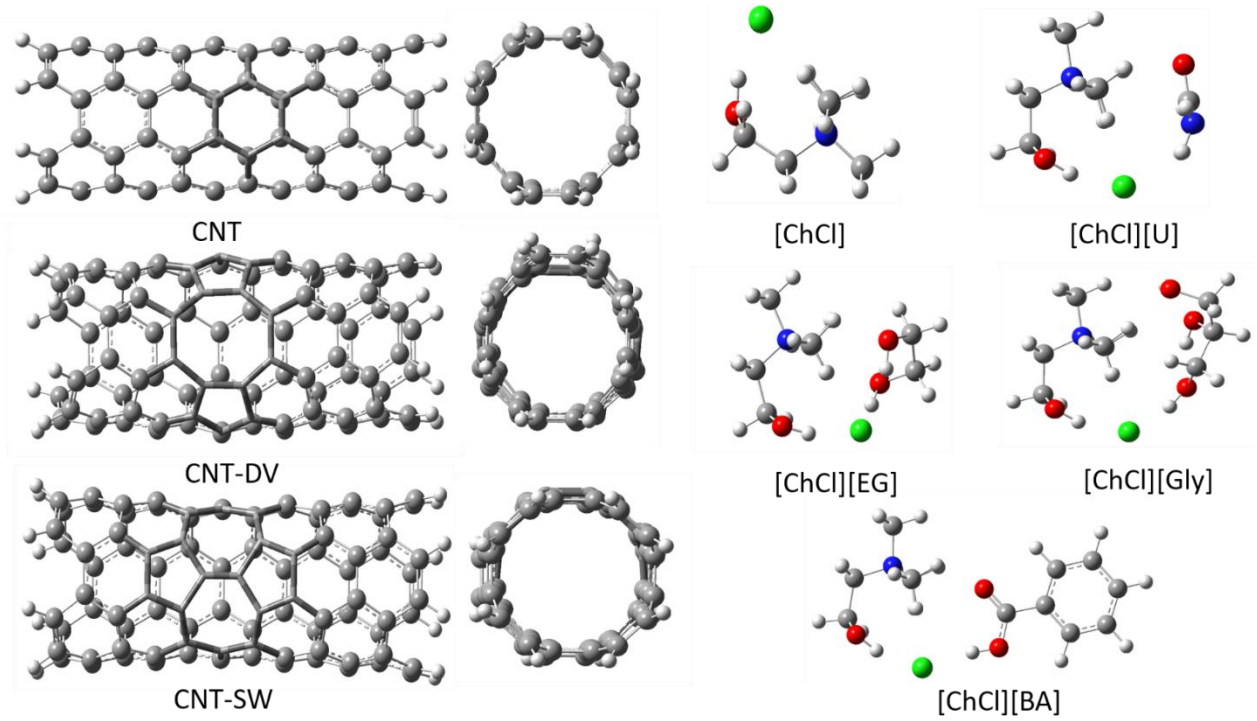

Figure 1. The most stable geometries of the CNT, CNT-DV, CNT-SW, [ChCl], [ChCl][U], [ChCl][EG], [ChCl][Gly], and [ChCl][BA] as calculated using M06-2X/cc-pVDZ. Both the side-on, and axis-on views are provided for the tubes.

In the optimized geometry of [ChCl] salt (Figure 1), the $[Cl]^-$ anion interacts with the $[Ch]^+$ cation through ion-ion and hydrogen bond (H-bond) interactions. The distance between the $[Cl]^-$ anion and $[Ch]^+$ cation in the [ChCl] geometry is shown by the H-bond interactions, including the C-H···$[Cl]^-$ (2.4 Å) and O-H···$[Cl]^-$ (2.1 Å) interactions.

A similar approach was used to find the most stable geometries of the [ChCl][U], [ChCl][EG], [ChCl][Gly], and [ChCl][BA] deep eutectic solvents. In this approach, based on the ESP maps of the [ChCl] salt and HBDs shown in Figure S1, several initial structures for each DES were built through the interaction of the regions with the positive and negative electrostatic potentials in the [ChCl] salt and the HBDs. In these regions, both the co-planar arrangements and

out-of-plane geometries for the interaction of [ChCl] salt with the HBDs were considered. Next, the initial structures were optimized at the M06-2X/cc-pVDZ level of theory and sorted according to their energies from the lowest to the highest. Finally, the geometries with the lowest energy were determined for each DES (Figure 1). We highlight some of the key structural characteristics of these complexes here, but again, for further information, please see our previous reports [28, 29]. The geometry of the [ChCl] salt in the DESs stays generally unchanged upon interaction with the HBDs. In the [ChCl][U] DES, the [U] molecule interacts with the [ChCl] salt through formation of N-H···$[Cl]^-$ (2.5 Å) H-bonds. In the case of [ChCl][EG] DES, both hydroxyl (-OH) groups in the [EG] molecule interact with the $[Cl]^-$ anion in the [ChCl] salt through the O-H···$[Cl]^-$ (2.2 Å) H-bonds. The [Gly] molecule interacts with the $[Cl]^-$ anion through one of its OH groups and forms the O-H···$[Cl]^-$ (2.1 Å) H-bond. In the [ChCl][BA] DES, the [BA] molecule interacts with the $[Cl]^-$ anion through its carboxyl (-COOH) group and forms COOH···$[Cl]^-$ (2.0 Å) H-bond.

3.2. Geometries and the nature of interaction of the adsorption of DESs on the CNT, CNT-DV and CNT-SW nanotubes

The adsorption of these DESs on the CNT, CNT-DV, and CNT-SW nanotubes occur from noncovalent interactions between the surfaces and different moieties of the DESs including the hydroxyl (OH) group, alkyl groups (methylene and methyl), and $[Cl]^-$ anion in the [ChCl] salt as well as the carbonyl (C=O) and amine (NH_2) groups in [U], OH groups and C-H bonds in the [EG] and [Gly], and carboxyl (COOH) and six-membered aromatic ring in the [BA]. The nature of the DES matters: the interactions are different for each. The electrostatic potential distribution of the sites in the DESs and the CNT, CNT-DV, and CNT-SW nanotubes are shown in Figure S1. To determine the initial structures for adsorption of DESs on the nanotubes, the DESs were placed in various positions and orientations above the native CNT and the defect sites in the CNT-DV and CNT-SW nanotubes. The constraint on the search was that the nearest atom distance of the DES to the nanotube was set at 2.7 Å. These initial structures were optimized at the M06-2X/cc-pVDZ level of theory and for each pair of molecules, ranked according to their energy from the lowest to the highest. Finally, the structures with the lowest energy for each DES@nanotube (DES = [ChCl][U], [ChCl][EG], [ChCl][Gly], and [ChCl][BA]) complex were determined (Figure 2).

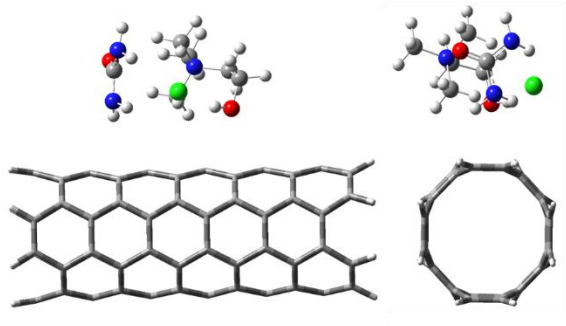

[ChCl][U]@CNT

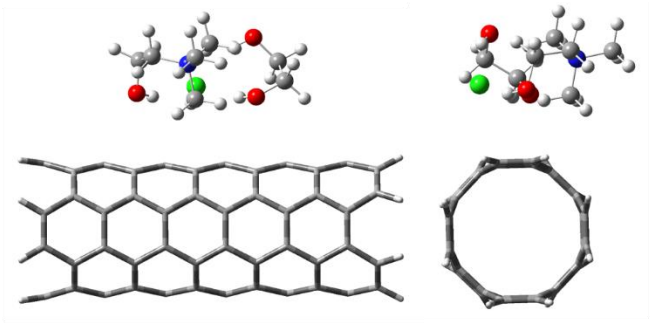

[ChCl][EG]@CNT

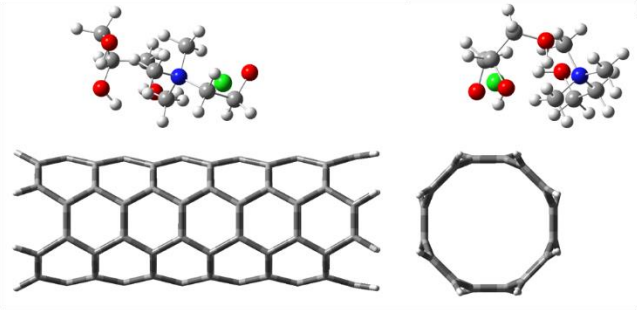

[ChCl][Gly]@CNT

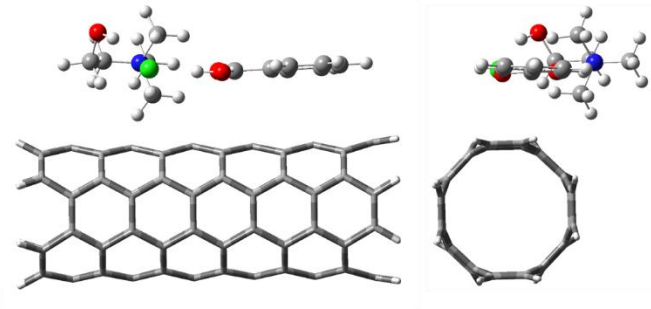

[ChCl][BA]@CNT

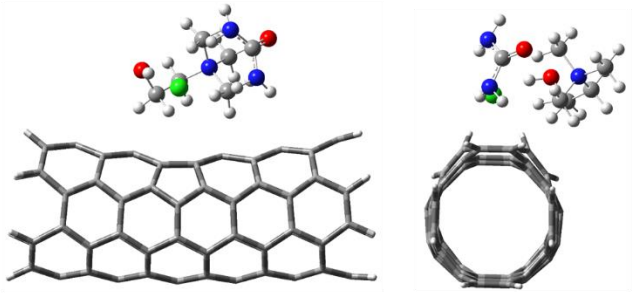

[ChCl][U]@CNT-DV

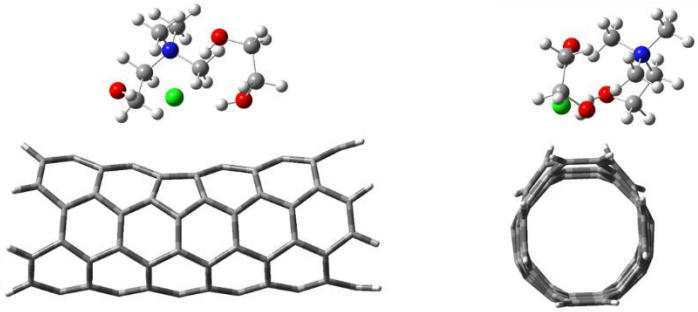

[ChCl][EG]@CNT-DV

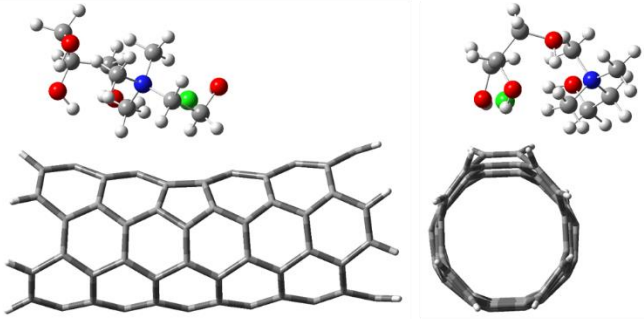

[ChCl][Gly]@CNT-DV

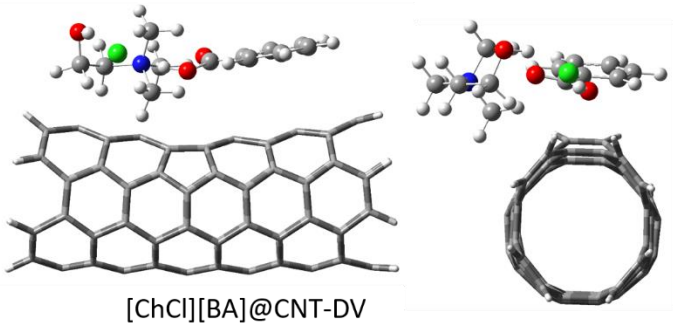

[ChCl][BA]@CNT-DV

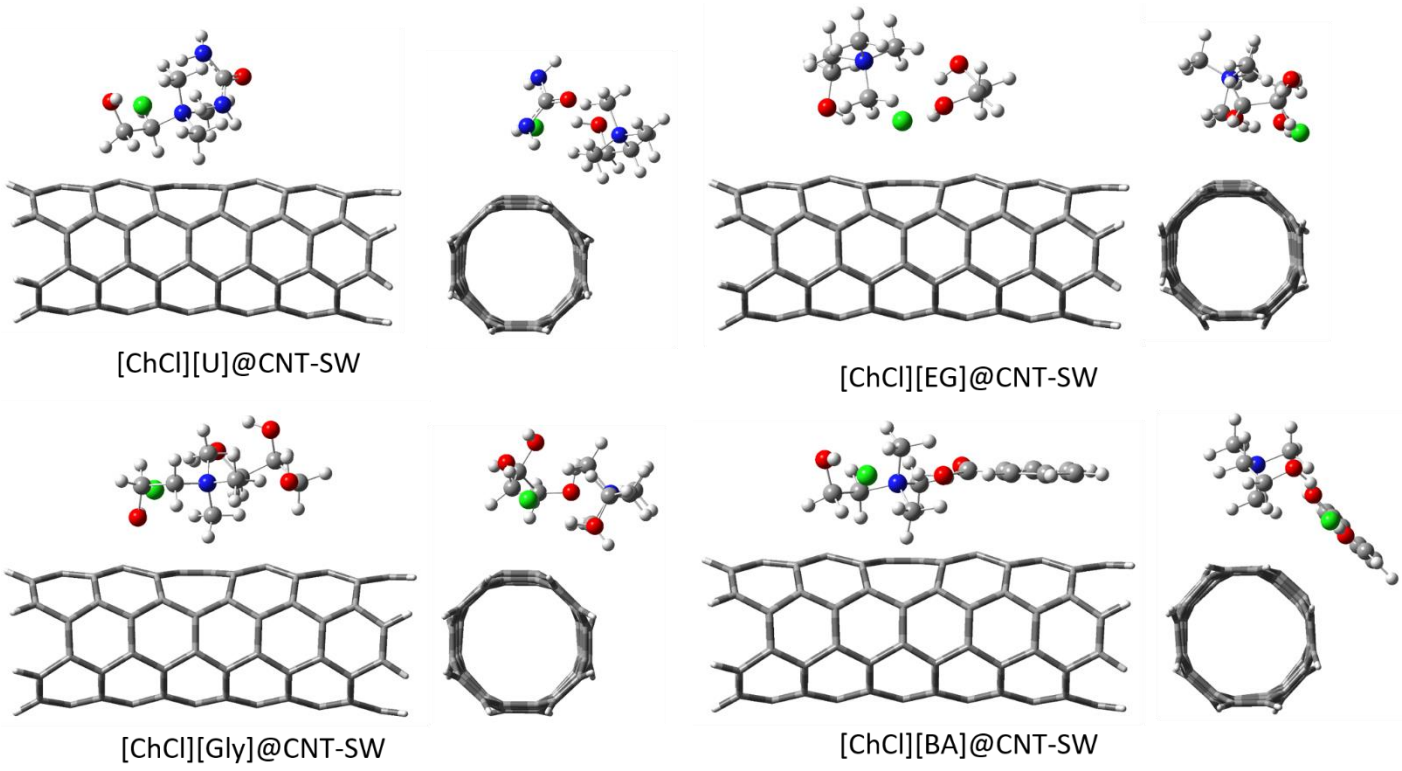

Figure 2. The most stable geometries for adsorption of DESs ([ChCl][U], [ChCl][EG], [ChCl][Gly], and [ChCl][BA]) on the CNT, CNT-DV, and CNT-SW surfaces, calculated at the M06-2X/cc-pVDZ level of theory.

As seen from the optimized geometries of [ChCl][U]@nanotube complexes in Figure 2, the N-H bond of urea is directed towards the nanotube surface to form a hydrogen bond. On the other hand, the [ChCl] salt in the DES interacts with the surface at the defect site through the strong dipoles of the C-H bonds of the ammonium or the $[Cl]^-$ anion. The arrangement of [ChCl][U] DES on these nanotube surfaces is similar to that on the graphene nanoflakes (GNFs) and GNFs containing double-vacancy (DV) and Stone-Wales (SW) defects and as reported in our previous study [42]. The nearest bond distances of the constituents of DESs, including the $[Ch]^+$ cation, $[Cl]^-$ anion, and [HBD] ([U], [EG], [Gly], and [BA]) from the CNT, CNT-DV, and CNT-SW surfaces are summarized in Table S1. As seen from the bond distances in the [ChCl][U]@nanotube complexes, the distance of [U] from the surface is shorter than that of the $[Ch]^+$ cation and $[Cl]^-$ anion, following the order $[Cl]^-$···nanotube> ($[Ch]^+$)C-H···nanotube> ([U])N-H···nanotube. This suggests that urea has a stronger interaction with the nanotube surfaces than the [ChCl] salt. For

the [ChCl][EG]@nanotube and the [ChCl][Gly]@nanotube complexes, the HBDs of [EG] and [Gly] interact with the surface via the oxygen atoms on the hydroxyl groups, and the [ChCl] salt interacts through $[Cl]^-$ and the C-H bonds of the methyl and methylene groups in the $[Ch]^+$ cation. In these complexes, the nearest bond distances between the [ChCl][EG] and [ChCl][Gly] DESs and the nanotube surfaces follow the order $[Cl]^-$···nanotube> ([EG]([Gly]))O···nanotube> $([Ch]^+)$C-H···nanotube. This order indicates that the $[Ch]^+$ cation has tighter interaction with the surfaces than the $[Cl]^-$ anion or the HBDs. In the case of [ChCl][BA]@nanotube complexes, the [ChCl][BA] DES interacts with the nanotube surfaces through the $[Cl]^-$ anion, the C-H bonds of methyl and methylene groups in the $[Ch]^+$ cation, the oxygen (O) atom in the COOH group of the [BA], and the π-π interactions between the six-membered aromatic ring in [BA] and the surfaces. In such complexes, the bond distance between the $[Ch]^+$ cation and the surfaces is shorter than that between the $[Cl]^-$ anion and the [BA] and the surfaces, following the order $[Cl]^-$···nanotube> ([BA])O···nanotube> $([Ch]^+)$C-H···nanotube. Again these interactions are similar to those we observed for graphene nanoflakes. The high degree of curvature of this surface does not greatly change how the DES interacts with the surface.

3.3. Adsorption energy and electronic properties of DES@nanotube complexes

The adsorption energy (E_{ads}) of DESs on the CNT, CNT-DV, and CNT-SW surfaces was used to evaluate the stability of the DES@nanotube complexes. The E_{ads} values for the complexes were calculated according to Equation 1 and are summarized in Table 1. Our calculations show that the E_{ads} values for the adsorption of DESs on the surfaces are negative, indicating that adsorption is favorable. The E_{ads} values for the DES@nanotube complexes are in the range of -9.48 to -17.48 kcal/mol. Our findings suggest that the presence of DV and SW defects on the CNT surface increases the adsorption strength of DESs on the CNT surface, following the order DES@CNT-SW > DES@CNT-DV > DES@CNT. In order to gain more insight into the DESs adsorption behavior on the nanotube surfaces, their E_{ads} values were compared. As seen from Table 1, the adsorption of DESs on the surfaces follows the order [ChCl][BA]@nanotube > [ChCl][Gly]@nanotube > [ChCl][U]@nanotube > [ChCl][EG]@nanotube. It is obvious that the [ChCl][BA] DES has the highest adsorption strength on the surfaces. The molar van der Waals volume (V_m) of the DESs was computed at the M06-2X/cc-pVDZ level of theory to determine the rationale for this observation. As seen from Table 1, the V_m values for the DESs follow the order [ChCl][BA] (191.34 cm^3/mol)> [ChCl][Gly] (170.44 cm^3/mol)> [ChCl][U] (157.22 cm^3/mol)>

[ChCl][EG] (148.22 cm^3/mol). [ChCl][Gly]'s higher V_m value over the [ChCl][EG] is likely due to [Gly] having more atoms, and consequently a larger surface area, than [EG], which leads to a higher number of van der Waals interactions with the surfaces. The V_m value for the [ChCl][U] is intermediate between the two as the weak [U] H-bonding interaction leads to greater V_m value for this DES with respect to [ChCl][EG]. In the case of [ChCl][BA], the presence of the flat phenyl ring and the associated substituents increases the size and V_m value of [ChCl][BA] with respect to other DESs and provides excellent opportunities for maximizing contact as they sit parallel to the surfaces in all cases, leading to higher van der Waals interactions in comparison with other HBDs. The order of V_m values for the DESs is in good agreement with the observed order for adsorption of DESs on the surfaces. Therefore, it can be concluded that the E_{ads} values of DESs on the surfaces increase with increasing molar van der Waals volume of the DESs. The greater the V_m values, the greater is the intermolecular noncovalent interactions between the DESs and the nanotube surfaces.

A comparison between the adsorption energies of DESs on these nanotube surfaces and those on the graphene nanoflake (GNF), hexagonal boron nitride nanoflake (h-BNNF) and their defective structures reported in our previous studies [28, 29] indicates that the DESs have a lower tendency to adsorption on the CNT, CNT-DV and CNT-SW nanotube surfaces than other nanoflakes. This could be due to the cylindrical topology of the CNT, CNT-DV and CNT-SW nanotubes in comparison to the flat structure of GNF, h-BNNF and their defective nanoflakes. In order to understand the role of DV and SW defects on the CNTs and GNFs surfaces in the adsorption of DESs, their E_{ads} values are compared in Figure 3. This comparison demonstrates that these defects behave differently in the adsorption of DESs on the GNFs and CNTs. As seen from Figure 3, the DV defects on the GNF surfaces have more tendency than SW defects for the adsorption of DESs, while the tendency to adsorption on the defective CNTs is reverse; the CNT-SW surface shows stronger adsorption than the CNT-DV surface. This could arise from significant differences in how the defects represent themselves on a curved vs. flat surface; the distortions of the local electronic structure are different.

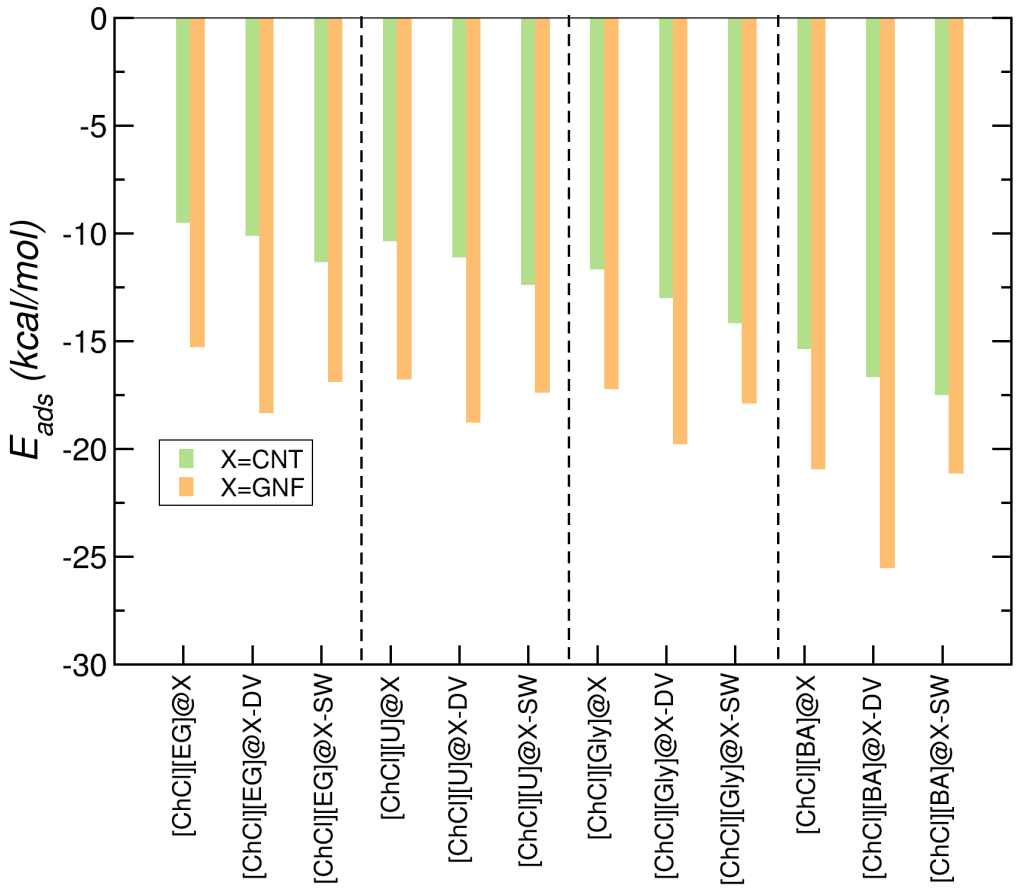

Figure 3. A comparison between the adsorption energies (E_{ads}) values for adsorption of DESs on the CNTs, graphene nanoflakes (GNFs) and their defective structures. The E_{ads} data (presented as binding energy (E_b)) for the DES@GNF, DES@GNF-DV and DES@GNF-SW complexes has been taken from our previous study [28].

To evaluate the charge transfer between the DESs and the nanotubes, the ChelpG charge analysis was performed on the DES@nanotube complexes. The charge transfer (Q_{CT}) values in the complexes were obtained by the calculation of ChelpG charge on the nanotube surfaces in the DES@nanotube complexes and are listed in Table 1. Our results indicate that the noncovalent adsorption of DESs on the surfaces leads to the change in the sum of atomic charges of the DESs and the surfaces. The positive sign of Q_{CT} values for the DES@nanotube complexes reveals that the charge transfer occurs from the nanotube surfaces to the DESs. It should be noted that the charge transfer in these complexes is in the opposite direction to that in the complexes of GNF, GNF-DV and GNF-SW surfaces with the DESs, reported in our previous study [28]. The magnitude is small, and the change in curvature is apparently sufficient to invert directionality.

Furthermore, the magnitude of charge transfer increases with the presence of DV and SW defects on the CNT and GNF surfaces. The magnitude of charge transfer in the DES@nanotube complexes follows the order Q_{CT} (DES@CNT-SW)> Q_{CT} (DES@CNT-DV)> Q_{CT} (DES@CNT), while the magnitude of charge transfer in the complexes of GNF, GNF-DV and GNF-SW surfaces with the DESs follows the order Q_{CT} (DES@GNF-DV)> Q_{CT} (DES@GNF-SW)> Q_{CT} (DES@GNF). These orders are consistent with the observed adsorption energy values for these complexes.

Table 1. The calculated adsorption energy (E_{ads} in kcal/mol), charge transfer (Q_{CT} in e), molar volume (V_m in cm^3/mol), the HOMO and LUMO energies (E_{HOMO} and E_{LUMO} in eV), HOMO-LUMO energy gap (E_g in eV) chemical hardness (η in eV) and dipole moment (D in Debye) of the nanotubes, DESs and DES@nanotube complexes.

Structure	E_{ads}	[a]Q_{CT}	V_m	E_{HOMO}	E_{LUMO}	[b]E_g	[c]η	D
CNT				-5.25	-2.59	2.66	1.330	0.00
CNT@DV				-5.59	-2.80	2.79	1.395	1.97
CNT@SW				-5.37	-2.53	2.84	1.420	2.15
[ChCl][EG]			148.22	-7.74	1.14	8.88	4.440	10.32
[ChCl][U]			157.22	-7.55	1.16	8.71	4.355	9.78
[ChCl][Gly]			170.44	-7.50	1.22	8.72	4.360	9.75
[ChCl][BA]			191.34	-7.61	-0.04	7.57	3.785	10.33
[ChCl][EG]@CNT	-9.48	0.3453		-5.07	-2.4	2.67	1.335	9.76
[ChCl][EG]@CNT-DV	-10.09	0.3468		-5.31	-2.52	2.79	1.395	9.34
[ChCl][EG]@CNT-SW	-11.31	0.3897		-5.17	-2.34	2.83	1.415	9.75
[ChCl][U]@CNT	-10.33	0.3562		-5.14	-2.48	2.66	1.330	8.53
[ChCl][U]@CNT-DV	-11.09	0.3880		-5.46	-2.73	2.73	1.365	8.16
[ChCl][U]@CNT-SW	-12.35	0.4300		-5.38	-2.5	2.88	1.440	8.03
[ChCl][Gly]@CNT	-11.63	0.3717		-5.12	-2.47	2.65	1.325	7.78
[ChCl][Gly]@CNT-DV	-12.98	0.3994		-5.43	-2.62	2.81	1.405	7.66
[ChCl][Gly]@CNT-SW	-14.13	0.4565		-5.24	-2.37	2.87	1.435	7.66
[ChCl][BA]@CNT	-15.34	0.3263		-5.11	-2.45	2.66	1.330	8.85
[ChCl][BA]@CNT-DV	-16.63	0.3445		-5.45	-2.71	2.74	1.370	8.96
[ChCl][BA]@CNT-SW	-17.48	0.3940		-5.26	-2.4	2.86	1.430	8.05

[a]Q_{CT} is the charge transfer values in the DES@nanotube complexes, resulting from the calculation of ChelpG charge on the nanotubes in the DES@nanotube complexes. The charge of the nanotubes is zero before the adsorption of DESs.

[b]$E_g = E_{LUMO} - E_{HOMO}$.

[c]$\eta = (E_{LUMO} - E_{HOMO})/2$.

The dipole moment (D) of molecules affects their solubility in polar media. The dipole moments of the DESs, nanotube, and the DES@nanotube complexes were calculated and are summarized in Table 1. The dipole moment of the CNT surface increases from 0.0 Debye to 1.97 Debye or 2.15 Debye with the presence of DV or SW defects on the CNT surface, respectively. The dipole moment of the nanotubes increases further with the adsorption of DESs due to charge transfer between the nanotubes and the DESs and further disruption of symmetry. It should be noted that the large value of dipole moments for the DES@nanotube complexes suggests these normally hydrophobic species could be solvated by water (D = 1.9 Debye). The calculation of dipole moment values for the DES@nanotube complexes shows that the polarity of the complexes follows the order [ChCl][EG]@nanotube > ChCl][BA]@nanotube > [ChCl][U]@nanotube > [ChCl][Gly]@nanotube. To reiterate, this predicts that [ChCl][EG]@nanotube complexes would have the highest solubility in polar media like water.

Frontier orbitals, including the highest occupied molecular orbital (HOMO) and the lowest unoccupied molecular orbital (LUMO), are used for the investigation of the effect of molecular adsorption on the properties of the surfaces. The HOMO-LUMO energy gap (E_g) property for a molecule is calculated based on the energy difference between the HOMO and LUMO orbitals ($E_g = E_{LUMO} - E_{HOMO}$). To understand the effect of DES adsorption on the E_g property of the surfaces, the HOMO energy, LUMO energy, and E_g value of the DESs, surfaces and the DES@nanotube complexes were calculated and listed in Table 1. The E_g value for the DESs is in the range of 7.57 eV – 8.88 eV. The E_g value of the CNT surface increases from 2.66 eV to 2.79 eV and 2.84 eV with the creation of DV and SW defects in the CNT surface, respectively. Our results show that the adsorption of DESs on the CNT, CNT-DV, and CNT-SW surfaces has a marginal effect on the E_g values of the surfaces. This is due to the weak van der Waals adsorption of DESs on the nanotube surfaces. Furthermore, it should be mentioned that the E_g values of the complexes resulted from adsorption of each DES on the CNT, CNT-DV and CNT-SW surfaces follow the order E_g (DES@CNT-SW)> E_g (DES@CNT-DV)> E_g (DES@CNT). For example, these values for the [ChCl][BA]@CNT-SW, [ChCl][BA]@CNT-DV, and [ChCl][BA]@CNT complexes are 2.86 eV, 2.74 eV, and 2.66 eV, respectively. The order observed above for the E_g values of the DES@nanotube complexes is in good agreement with the observed trend of their E_{ads} values, E_{ads} (DES@CNT-SW)> E_{ads} (DES@CNT-DV)> E_{ads} (DES@CNT).

The calculated E_g values for the DESs, CNT, CNT-DV, CNT-SW surfaces and the DES@nanotube complexes are related to their chemical hardness ($\eta = E_{LUMO} - E_{HOMO}/2$) values. According to the η values summarized in Table 1, the η values of course follow the same trend observed for the E_g and E_{ads}. The DES@CNT-SW complexes have the highest chemical hardness, stability, and hence the lowest expected chemical reactivity.

3.4. Noncovalent interaction analysis in the DES@nanotube complexes

The noncovalent interaction (NCI) analysis and energy decomposition analysis (EDA) were performed on the DES@nanotube complexes to highlight the role of noncovalent interactions in the adsorption of DESs on surfaces. In the NCI analysis, the 3D graphics of reduced density gradient (*RDG*) and the 2D scatter plot of *RDG* versus $sign(\lambda_2)\rho(r)$ are plotted (Figure S2). The term $sign(\lambda_2)\rho(r)$ represents the electron density ($\rho(r)$) into the sign of second Hessian eigenvalues (λ_2). The 2D scatter plot is visualized to determine the type of noncovalent interactions which are responsible for the adsorption of DESs on the surfaces. In the 2D scatter plots, the points which are located in the regions with $sign(\lambda_2)\rho(r) < 0$ show strong interactions such as electrostatic interactions and hydrogen bonding interactions. More negative values for the peak position in the 2D scatter plot indicate stronger attractive interactions. The van der Waals (vdW) interactions as weak interactions are found in the regions with the $sign(\lambda_2)\rho(r) \approx 0$. In addition, the repulsion interactions such as steric effects are observed in the regions with $sign(\lambda_2)\rho(r) > 0$ [48]. It should be mentioned that the strength of the interactions is related to the $sign(\lambda_2)\rho(r)$ term. The strength of interactions is shown by the colors in the 2D scatter plots and the 3D graphics of *RDG* (Figure S2). The strong attractive interactions, weak attractive interactions, and repulsive interactions are shown in blue, green, and red respectively [48]. Although the strength of the interactions is presented by the colors in the 2D scatter plots, more information about the type of the interacting atoms associated with the colors can not be visualized from the 2D scatter plots. Therefore, the 3D graphics of RDG are plotted to show the relationship between the type of interacting atoms and the strength of their interactions in the molecular systems. In addition, it should be mentioned that large numbers of dots (large dot densities) in the regions with $sign(\lambda_2)\rho(r) < 0$ in the 2D scatter plots represent the regions of most significant interactions in the studied systems.

As seen from Figure S2, only a blue peak in the regions with $sign(\lambda_2)\rho(r) < 0$ (about -0.03 a.u) is seen in the 2D scatter plots of [ChCl][U]@nanotube complexes. According to the RDG plots, this

peak is related to the ([Ch]$^+$)O-H···[Cl]$^-$ H-bond interaction in the [ChCl][U] DES. In addition to this peak, other new peaks appear in the regions with $sign(\lambda_2)\rho(r) < 0$ in the 2D scatter plots of the DES@nanotube (DES: [ChCl][EG], [ChCl][Gly] and [ChCl][BA]) complexes. As seen from Figure S2, a blue peak with $sign(\lambda_2)\rho(r)$ values less than -0.03 a.u. is seen in the 2D scatter plots of the [ChCl][EG]@nanotube and [ChCl][Gly]@nanotube complexes. The RDG plots reveal that this new peak is associated with the ([EG])O-H···[Cl]$^-$ and ([Gly])O-H···[Cl]$^-$ H-bond interactions. The $sign(\lambda_2)\rho(r)$ values less than -0.03 a.u. for these interactions confirm that they are weaker than the ([Ch]$^+$)O-H···[Cl]$^-$ H-bond interactions. Furthermore, for the [ChCl][BA]@nanotube complexes, the new blue peak is seen with $sign(\lambda_2)\rho(r)$ values more than -0.03 a.u. (about -0.04 a.u.). The RDG plots show that this peak is associated with the ([BA])COOH···[Cl]$^-$ H-bond interactions. According to the $sign(\lambda_2)\rho(r)$ values for these interactions, we find that the ([BA])COOH···[Cl]$^-$ H-bond interactions in the [ChCl][BA]@nanotube complexes are stronger than ([EG])O-H···[Cl]$^-$ and ([Gly])O-H···[Cl]$^-$ H-bond interactions in the [ChCl][EG]@nanotube and [ChCl][Gly]@nanotube complexes.

The weak attractive interactions are primarily associated with the interactions between the DESs and the surfaces, including [Cl]$^-$···nanotube, ([U])N-H···nanotube, ([EG] and [Gly])O-H···nanotube, ([BA])COOH···nanotube, C-H···nanotube, and π-π stacking interactions. This result shows that the interaction between the DESs and surfaces is weak and that vdW interactions are primarily responsible for the adsorption of DESs on the surfaces. A notable interaction is seen when the [ChCl][BA] is adsorbed on the surfaces. In the [ChCl][BA]@nanotube complexes, the HBD of [BA] has a parallel arrangement with the surfaces and is stabilized by the interaction of its aromatic ring with the surfaces through π-π stacking interactions. These interactions enhance the adsorption strength of [ChCl][BA] DES on the surfaces and result in an increase in the adsorption energy values of [ChCl][BA]@nanotube complexes with respect to other complexes.

The interaction energy between two fragments can be interpreted by the energy decomposition analysis (EDA) method, which was developed by Morokuma [49] and by Ziegler and Rauk [50]. In this method, the interaction energy between two fragments (ΔE_{int}) is partitioned into four meaningful components, including a repulsive term (ΔE_{Pauli}) and three attractive terms (ΔE_{elec}, ΔE_{orb} and ΔE_{disp}):

1) the repulsive exchange (Pauli) energy between electrons of the two fragments with the same spin (ΔE_{Pauli}); 2) the electrostatic interaction energy between the charge densities of the two

fragments (ΔE_{elec}); 3) the energy related to the orbital mixing of the fragments (ΔE_{orb}); and 4) the energy related to the attractive forces between the induced dipoles of interacting species (dispersion energy (ΔE_{disp})) [49, 50]. The results of EDA for the DES@nanotube complexes, calculated at the PBE-D3/TZP level of theory, are summarized in Table S2 and shown in Figure 4. The PBE-D3/TZP method was also used in our previous works to find the contribution of attractive interactions in the adsorption of ionic liquids and DESs on the graphene nanoflakes and their defects [28,29,36-38,32] as well as ionic liquids on the nitrogen-doped graphene nanoflakes [41] and hexagonal boron-nitride nanoflakes [39].

The interaction energy (ΔE_{int}) values between the DESs and the CNT, CNT-DV, and CNT-SW surfaces, which are resulted from the sum of the four components track the E_{ads} as expected, and range from -7.76 to -17.58 kcal/mol. The repulsion term of ΔE_{Pauli} has a positive sign, while the attractive terms of ΔE_{elec}, ΔE_{orb}, and ΔE_{disp} have a negative sign and favor adsorption. In order to understand the role of attractive contributions on the adsorption of DESs on the surfaces, the percent contribution of each attractive term to the interaction energy between the DESs and the surfaces was calculated according to Equation 2.

$$\Delta E_x(\%) = (\Delta E_x/(\Delta E_{elec} + \Delta E_{orb} + \Delta E_{disp})) \times 100 \quad \text{(Equation 2)}$$

In this equation, the ΔE_x term corresponds to one of the three attractive terms of ΔE_{elec}, ΔE_{orb}, and ΔE_{disp}.

As seen from the percent contribution of attractive terms listed in Table S2, the magnitude of the percent contributions in the DES@nanotube complexes follows the order $\Delta E_{disp} > \Delta E_{elec} > \Delta E_{orb}$. This result reveals that the contribution of dispersion interactions in the adsorption of DESs on the surfaces is greater than that of electrostatic interactions and orbital interactions. For example, the percent contribution of ΔE_{disp} for the CNT-SW@[ChCl][BA] complex is 43.5% and higher than that of ΔE_{elec} (32.0%) and ΔE_{orb} (24.5%) terms. We also found that the observed trend for the attractive terms is in good agreement with the previous results for adsorption of ionic liquids and DESs on the graphene nanoflakes and their defects [28, 38] as well as ionic liquids on the nitrogen-doped graphene nanoflakes [41] and hexagonal boron-nitride nanoflakes [39].

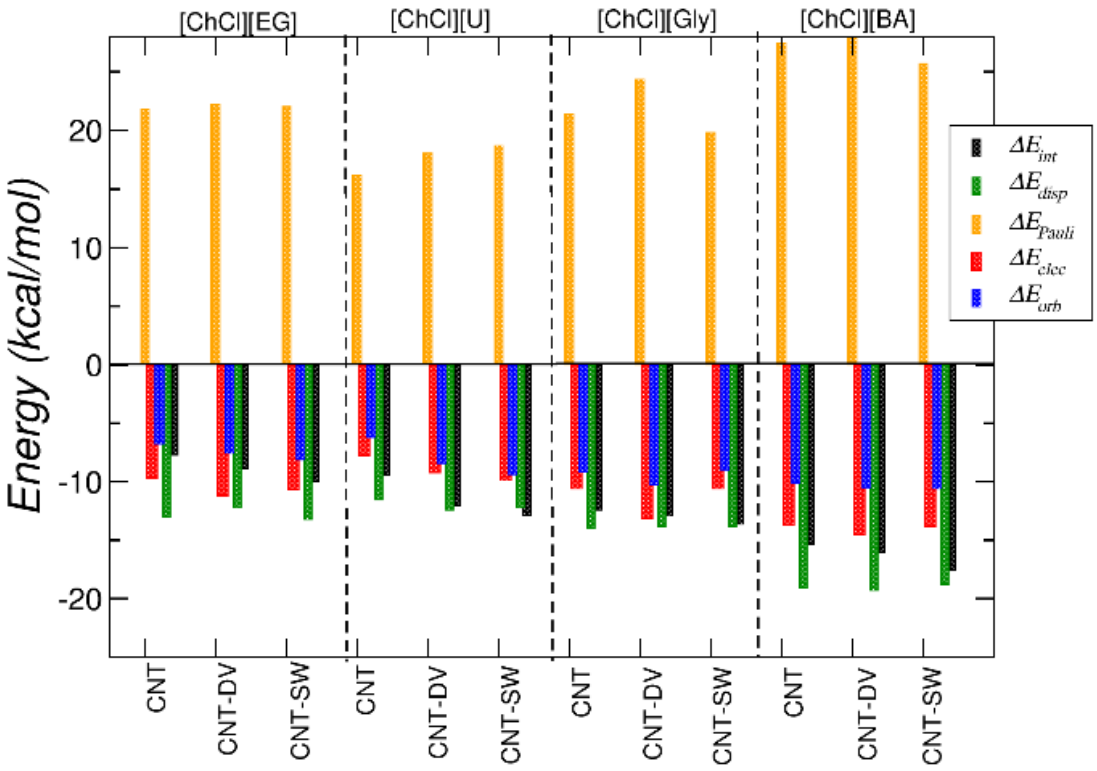

Figure 4. The results of energy decomposition analysis (EDA, in kcal/mol) of the DES@nanotube complexes, calculated at the PBE-D3/TZP level of theory.

3.5. UV-Vis absorption spectra of the DES@nanotube complexes

The UV-visible absorption spectra of the CNT, CNT-DV, CNT-SW surfaces and their complexes with the DESs were calculated at the TD-M06-2X/cc-pVDZ level of theory and are shown in Figure 5. The optical properties associated with the main transitions in the absorption spectra, including wavelengths (λ), excitation energies (E), oscillator strength (f), excitation coefficients, and excitation states (n) are summarized in Table S3. As seen from Figure 5, the CNT, CNT-DV, and CNT-SW surfaces all show their absorption peaks within the visible region of the energy spectrum, which means that these materials are suitable candidates for colorimetric and fluorescent sensors [56-58]. According to our results, the UV-visible absorption spectrum of the CNT surface shows an intensive absorption peak at λ = 559 nm corresponding to the electronic transition HOMO → LUMO+1, which corresponds to $\pi \rightarrow \pi^*$ electronic transitions in the benzene

rings of the CNT surface. This result is in good agreement with the experimental results reported in the literature [59].

The presence of DV and SW defects in the CNT surface shifts the absorption peak of CNT and induces the emergence of new peaks. The UV-visible absorption spectrum of the CNT-DV surface shows two absorption peaks at λ = 516 nm and λ = 714 nm, which correspond to $\pi \rightarrow \pi^*$ electronic transitions. The most intense absorption peak, which shows a lower wavelength at λ = 516 nm is attributed to the electronic transition HOMO-3→LUMO. The second peak with a lower intensity (λ = 714 nm) corresponds to the electronic transition HOMO-1→LUMO+1. In the case of CNT-SW surface, the main absorption peak (λ = 584 nm, HOMO→LUMO+2) is observed about 25 nm higher than the observed absorption peak in the CNT spectrum (λ = 559 nm, HOMO→LUMO+1). In addition, a new peak with a lower intensity appears at λ = 671 nm, attributed to the electronic transition HOMO→LUMO+2.

To gain insight into the effect of DES adsorption on the spectral properties of the surfaces, the absorption spectra of the DES@nanotube complexes were computed. Figure 5 shows that the absorption spectra of DES@nanotube complexes are similar in shape to those of CNT, CNT-DV, and CNT-SW surfaces, indicating that the DES adsorption has a marginal effect on the main absorption peaks of the surfaces. In addition, only a small change is seen in the intensity of absorption peak of CNT-SW surface at λ = 671 nm upon adsorption of DESs. The small effect of DES adsorption on the absorption spectra and optical behavior of the surfaces is further evidence that the adsorption of DESs onto the surfaces is weak. This is in contrast to adsorption onto the flat nanosheets of the graphene or the boron nitride where the changes in optical activity were noticeable [28, 38]. In those cases, the adsorption of DESs and ionic liquids was stronger and showed more covalent character. In this case the disruption of the curved surface is minimal.

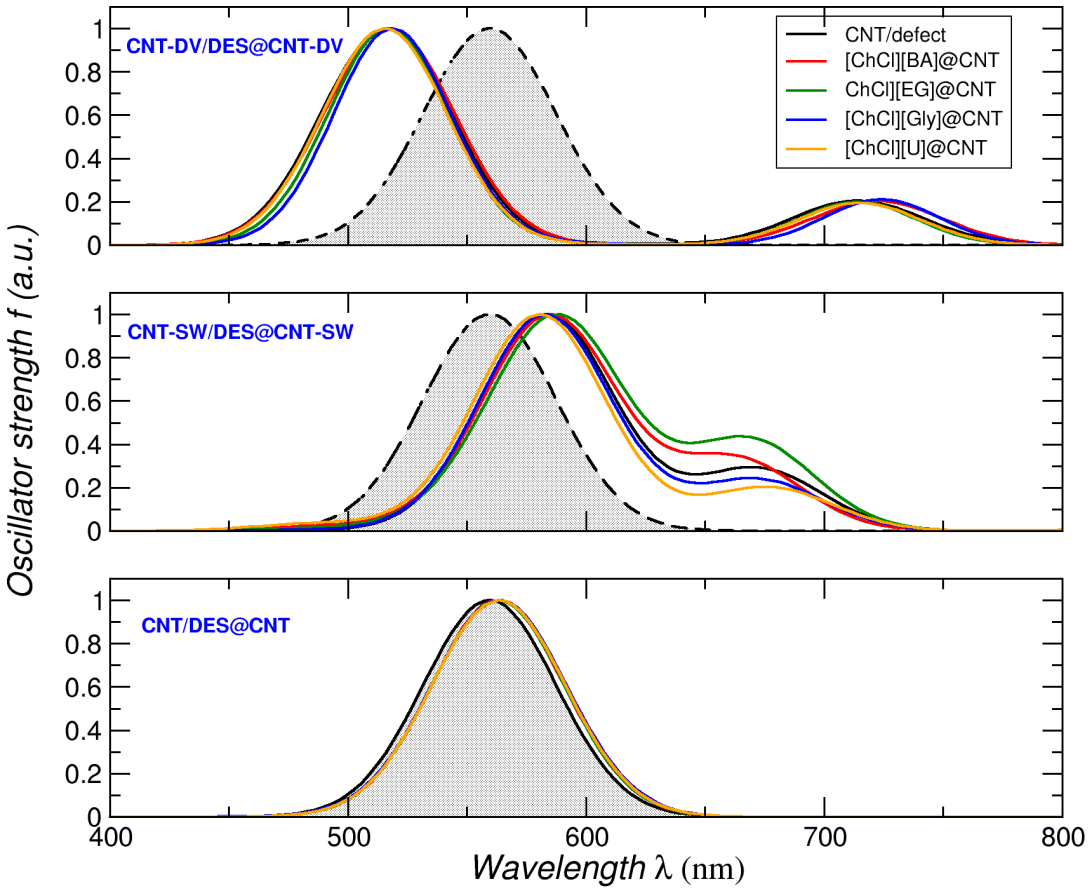

Figure 5. The UV-visible absorption spectra of CNT, CNT-DV, CNT-SW surfaces and their complexes with DESs, calculated at the TD-M06-2X/cc-pVDZ level of theory.

In order to understand how the charge transfer occurs via the excited states, the transition density matrix (TDM) heat maps are used. TDM heat maps are based on the self-defined fragments and interpreted based on a self-defined fragment index of electron transfer. For TDM heat maps, the DES@nanotube complexes were divided into three fragments including fragment 1 (CNT, CNT-DV, and CNT-SW), fragment 2 ([ChCl]), and fragment 3 (HBDs of [EG], [U], [Gly], and [BA]). TDM heat maps for the main excited states in all the DES@nanotube complexes are presented in Figure S3 and shown for the [ChCl][BA]@nanotube complexes in Figure 6.

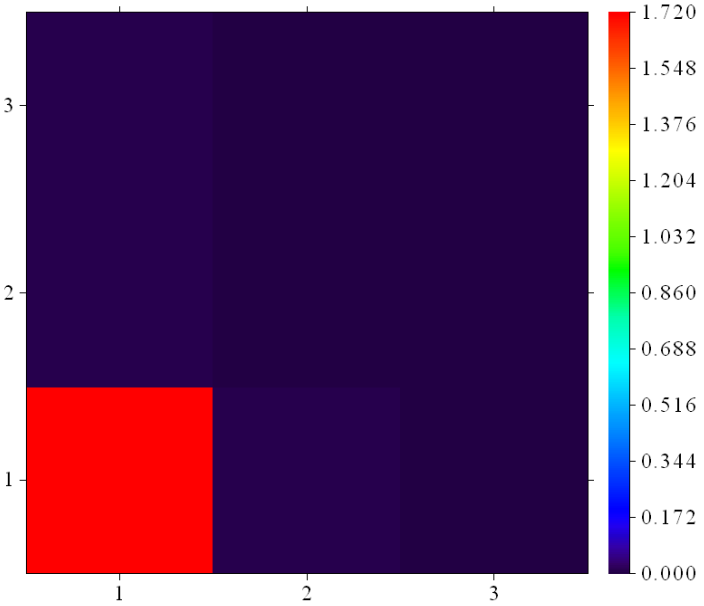

[ChCl][BA]@CNT (S0 → S4)

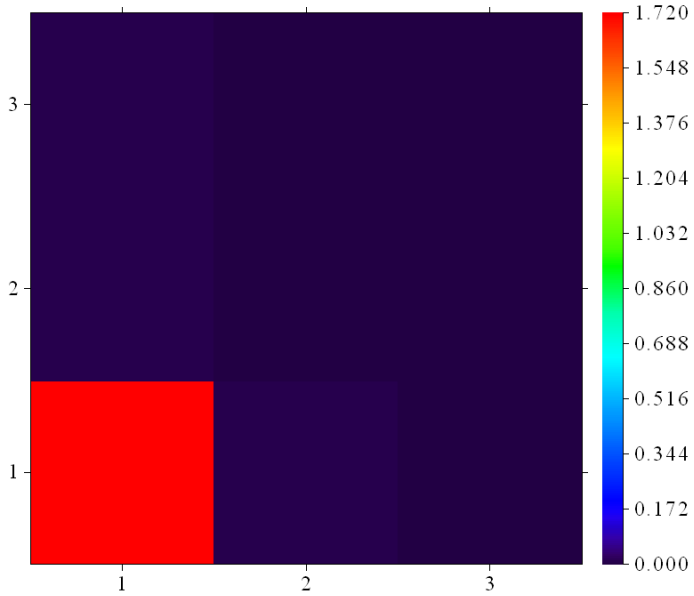

[ChCl][BA]@CNT-DV (S0 → S4)

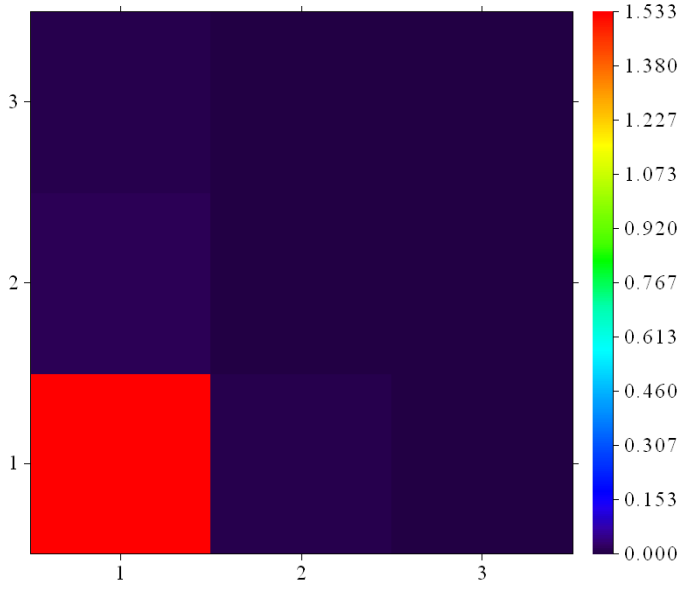

[ChCl][BA]@CNT-DV (S0 → S8)

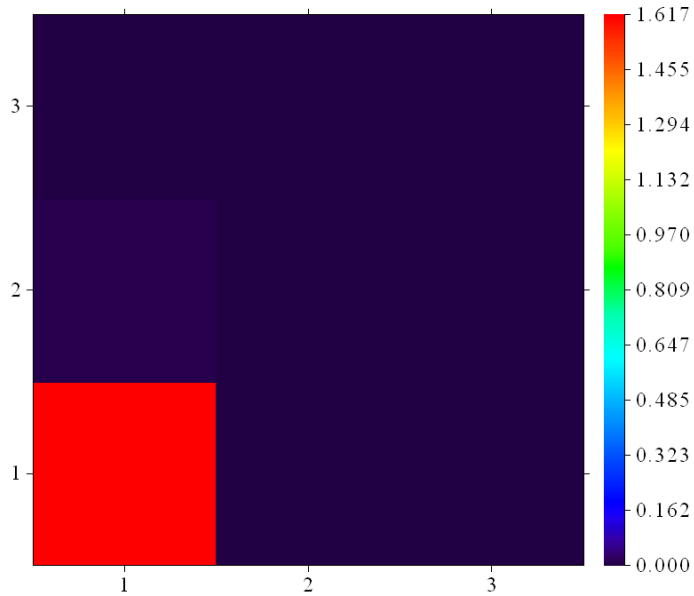

[ChCl][BA]@CNT-SW (S0 → S4)

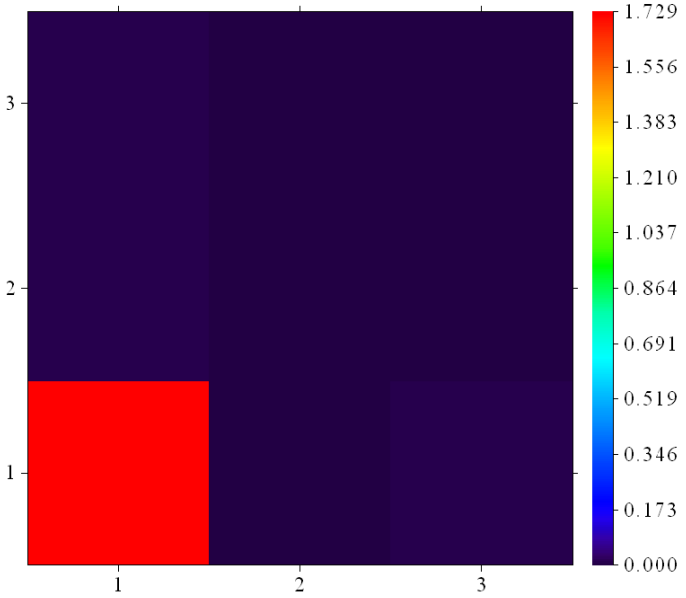

[ChCl][BA]@CNT-SW (S0 → S6)

Figure 6. The TDM heat maps for the main excited states in the [ChCl][BA]@nanotube complexes. 1, 2 and 3 terms in the x and y axes are the surfaces (CNT, CNT-DV and CNT-SW), [ChCl] and [BA], respectively. The TDM heat maps for the other species are provided as Figure S3 in the supporting information. In these maps, the x and y axes are the receiving and originating fragments for the main excited states, respectively.

The charge transferred between the CNT, CNT-DV, and CNT-SW surfaces and the DESs for the main excited states is also calculated and listed in Table S4. As seen from Table S4, no charge transfer for the main excited states is observed between the [ChCl] and the HBDs, while it occurs between the surfaces and the DESs. As seen from Figure S3 and Figure 6, the magnitude of diagonal elements (the red boxes) in the TDM heat maps of all the DES@nanotube complexes is more significant than that of the off-diagonal elements (the blue boxes). This reveals that an important electron transfer does not occur through inter fragment excited states. The red boxes in the TDM heat maps show that the electrons and holes are mainly localized on the CNT, CNT-DV and CNT-SW surfaces (fragment 1) in the DES@nanotube complexes. This means that the charge transfer related to the main transition states occurs mostly in the CNT, CNT-DV and CNT-SW surfaces. This finding is consistent with the TDDFT results of DES@nanotube complexes that no

significant change was observed in the absorption spectra of the surfaces with adsorption of DESs; significant charge transfer through the excited states would change the absorption spectra. A similar result was observed in our previous study [29] for adsorption of the same DESs on the hexagonal boron nitride nanoflake (h-BNNF) and h-BNNF containing nitrogen and boron defects (B_{vac}-h-BNNF and N_{vac}-h-BNNF). In these complexes, the TDM heat maps showed that the excited states are generally related to the local excitation on the h-BNNF, B_{vac}-h-BNNF and N_{vac}-h-BNNF surfaces, which corresponds to the $\pi \rightarrow \pi^*$ transitions.

4. Conclusions

In this work, a DFT study was performed to investigate the interaction of deep eutectic solvents (DESs) with CNT, CNT-DV, and CNT-SW surfaces at the M06-2X/cc-pVDZ level of theory. These DESs are formed from two components of choline chloride ([ChCl]) as hydrogen bond acceptor (HBA) and urea ([U]), ethylene glycol ([EG]), glycerol ([Gly]), and benzoic acid ([BA]) as hydrogen bond donor (HBD). Noncovalent interaction (NCI) plots show that the adsorption of DESs on the surfaces occurs via van der Waals (vdW) interactions. The results of the NCI plots are further confirmed by the energy decomposition analysis (EDA), which shows that the percent contribution of dispersion interactions in the adsorption of DESs on the surfaces is greater than that of electrostatic interactions and orbital interactions.

The adsorption of DESs on the surfaces leads to a small charge transfer from the surfaces to the DESs. The calculation of adsorption energy (E_{ads}) values for the DES@nanotube complexes shows that the tendency of the DESs for adsorption on the CNT surface increases in the presence of DV and SW defects and follows the order E_{ads}(DES@CNT-SW)> E_{ads}(DES@CNT-DV)> E_{ads}(DES@CNT). The HOMO-LUMO energy gap (E_g) and chemical hardness (η) of the complexes also follow the same order observed for E_{ads} values, indicating that the DES@CNT-SW complexes have the lowest chemical reactivity. The E_{ads} values are associated with the volume of DES adsorbed on the surfaces. The greater the volume of DES, the greater both the number of noncovalent interactions between the DESs and the surfaces, and the E_{ads} values.

It should be noted that the [ChCl][BA] DES has the maximum adsorption energy due to the presence of the six-membered aromatic ring in the [BA] and its π-π interaction with the surfaces. Furthermore, because the main transition states in the DES@nanotube complexes occur mostly in the CNT, CNT-DV, and CNT-SW surfaces, the UV-visible absorption spectra and the

transition density matrix (TDM) heat maps show that there is no significant change in the absorption spectra of the surfaces with DESs adsorption.

A comparison between the adsorption properties of DESs on the nanotubes and the GNF surfaces and their defective structures indicates that the adsorption of DESs on the nanotubes is weaker than GNF and GNF-DV and GNF-SW surfaces. This leads to the observation of a marginal effect on the UV-visible absorption spectra of the CNT, CNT-DV and CNT-SW surfaces with respect to the GNF, GNF-DV and GNF-SW surfaces. DES binding can certainly occur to these nanotubes, and this could help solvate them, but it has a minimal effect on the properties of the tubes themselves.

Acknowledgements: We gratefully acknowledge financial support from the Research Council of Jahrom University, the Birjand University of Technology, and the University of Windsor. The authors declare that they have no competing financial interests.

Supporting Information: Additional tables of data, figures, and computational details are available in the accompanying supporting information file.

References

[1] C. Florindo, F. Lima, B.D. Ribeiro, I.M. Marrucho, Deep eutectic solvents: overcoming 21st century challenges, Curr. Opin. Green Sustain. Chem. 18 (2019) 31-36.

[2] H. Mizuuchi, V. Jaitely, S. Murdan, A.T. Florence, Room temperature ionic liquids and their mixtures: Potential pharmaceutical solvents, Eur. J. Pharm. Sci. 33 (2008) 326-331.

[3] A.P. Abbott, G. Capper, D.L. Davies, H.L. Munro, R.K. Rasheed, V. Tambyrajah, Preparation of novel, moisture-stable, Lewis-acidic ionic liquids containing quaternary ammonium salts with functional side chains, ChemComm. (2001) 2010-2011.

[4] M.M. Santos, L.C. Branco, Ionic Liquids and Deep Eutectic Solvents for Application in Pharmaceutics, Pharmaceutics. 12 (2020) 909.

[5] M. Hayyan, M.A. Hashim, A. Hayyan, M.A. Al-Saadi, I.M. AlNashef, M.E.S. Mirghani, O.K. Saheed, Are deep eutectic solvents benign or toxic?, Chemosphere. 90 (2013) 2193-2195.

[6] Q. Wen, J.-X. Chen, Y.-L. Tang, J. Wang, Z. Yang, Assessing the toxicity and biodegradability of deep eutectic solvents, Chemosphere. 132 (2015) 63-69.

[7] R. Costa, C.M. Pereira, A.F. Silva, Role of the anion on the Interfacial Structure of Ionic Liquids Binary Mixtures at Mercury Interfaces, Electrochim. Acta. 195 (2016) 150-157.
[8] F. Buchner, K. Forster-Tonigold, B. Uhl, D. Alwast, N. Wagner, H. Farkhondeh, A. Groß, R.J. Behm, Toward the Microscopic Identification of Anions and Cations at the Ionic Liquid|Ag(111) Interface: A Combined Experimental and Theoretical Investigation, ACS Nano. 7 (2013) 7773-7784.
[9] M. Zabihinpour, H.R. Ghenaatian, A novel multilayered architecture of graphene oxide nanosheets for high supercapacitive performance electrode material, Synth. Met. 175 (2013) 62-67.
[10] P.K. Sharma, S. Dorlikar, P. Rawat, V. Malik, N. Vats, M. Sharma, J.S. Rhyee, A.K. Kaushik, in: K.R. Khondakar, A.K. Kaushik (Eds.), Nanotechnology in Cancer Management, Elsevier, 2021, p. 1-33.
[11] H.-G. Liao, Y.-X. Jiang, Z.-Y. Zhou, S.-P. Chen, S.-G. Sun, Shape-Controlled Synthesis of Gold Nanoparticles in Deep Eutectic Solvents for Studies of Structure–Functionality Relationships in Electrocatalysis, Angew. Chem. Int. Ed. 47 (2008) 9100-9103.
[12] Y. Liu, J.B. Friesen, J.B. McAlpine, D.C. Lankin, S.-N. Chen, G.F. Pauli, Natural Deep Eutectic Solvents: Properties, Applications, and Perspectives, J. Nat. Prod. 81 (2018) 679-690.
[13] A. Abo-Hamad, M. Hayyan, M.A. AlSaadi, M.A. Hashim, Potential applications of deep eutectic solvents in nanotechnology, Chem. Eng. Sci. 273 (2015) 551-567.
[14] S. Iijima, Helical microtubules of graphitic carbon, Nature. 354 (1991) 56-58.
[15] H.R. Ghenaatian, M. Shakourian-Fard, G. Kamath, The effect of sulfur and nitrogen/sulfur co-doping in graphene surface on the adsorption of toxic heavy metals (Cd, Hg, Pb), J. Mater. Sci. 54 (2019) 13175-13189.
[16] S.A. Reyes, A. Struck, S. Eggert, Lattice defects and boundaries in conducting carbon nanotubes, Phys. Rev. B. 80 (2009) 075115.
[17] M. Bockrath, W. Liang, D. Bozovic, J.H. Hafner, C.M. Lieber, M. Tinkham, H. Park, Resonant Electron Scattering by Defects in Single-Walled Carbon Nanotubes, Science. 291 (2001) 283-285.
[18] L.A. Algharagholy, Defects in Carbon Nanotubes and their Impact on the Electronic Transport Properties, J. Electron. Mater. 48 (2019) 2301-2306.

[19] S. Baldo, V. Scuderi, L. Tripodi, A. La Magna, S.G. Leonardi, N. Donato, G. Neri, S. Filice, S. Scalese, Defects and gas sensing properties of carbon nanotube-based devices, J. Sens. Sens. Syst. 4 (2015) 25-30.
[20] N.M. Shaalan, O. Saber, F. Ahmed, A. Aljaafari, S. Kumar, Growth of Defect-Induced Carbon Nanotubes for Low-Temperature Fruit Monitoring Sensor, Chemosensors. 9 (2021) 131.
[21] M.K. AlOmar, M.A. Alsaadi, M. Hayyan, S. Akib, M.A. Hashim, Functionalization of CNTs surface with phosphonuim based deep eutectic solvents for arsenic removal from water, Appl. Surf. Sci. 389 (2016) 216-226.
[22] L. Chen, J. Deng, Y. Song, S. Hong, H. Lian, Highly Stable Dispersion of Carbon Nanotubes in Deep Eutectic Solvent for the Preparation of CNT-Embedded Carbon Xerogels for Supercapacitors, ChemElectroChem. 6 (2019) 5750-5758.
[23] Y.Y. Chen, R. Walvekar, M. Khalid, K. Shahbaz, T.C.S.M. Gupta, Stability and thermophysical studies on deep eutectic solvent based carbon nanotube nanofluid, Mater. Res. Express. 4 (2017) 075028.
[24] R. Walvekar, Y.Y. Chen, R. Saputra, M. Khalid, H. Panchal, D. Chandran, N.M. Mubarak, K.K. Sadasivuni, Deep eutectic solvents-based CNT nanofluid – A potential alternative to conventional heat transfer fluids, J. Taiwan. Inst. Chem. Eng. 128 (2021) 314-326.
[25] G.M. Verkhivker, Molecular dynamics simulations and modelling of the residue interaction networks in the BRAF kinase complexes with small molecule inhibitors: probing the allosteric effects of ligand-induced kinase dimerization and paradoxical activation, Mol. Biosyst. 12 (2016) 3146-3165.
[26] M. Atilhan, L.T. Costa, S. Aparicio, Elucidating the Properties of Graphene–Deep Eutectic Solvents Interface, Langmuir. 33 (2017) 5154-5165.
[27] S. Rozas, M. Atilhan, S. Aparicio, Insights on (C, BN, Si, Ge, MoS2) Nanotubes in Reline Deep Eutectic Solvent, J. Phys. Chem. B. 124 (2020) 3556-3567.
[28] M. Shakourian-Fard, S.M. Taimoory, H.R. Ghenaatian, G. Kamath, J.F. Trant, A DFT study of the adsorption of deep eutectic solvents onto graphene and defective graphene nanoflakes, J. Mol. Liq. 327 (2021) 114850.
[29] M. Shakourian-Fard, S. Maryamdokht Taimoory, H.R. Ghenaatian, G. Kamath, J.F. Trant, Effect of mono-vacant defects on the adsorption properties of deep eutectic solvents onto hexagonal boron-nitride nanoflakes, J. Mol. Liq. 349 (2022) 118122.

[30] J.A. Sirviö, M. Visanko, H. Liimatainen, Deep eutectic solvent system based on choline chloride-urea as a pre-treatment for nanofibrillation of wood cellulose, Green Chem., 17 (2015) 3401-3406.
[31] A.R. Harifi-Mood, R. Buchner, Density, viscosity, and conductivity of choline chloride+ethylene glycol as a deep eutectic solvent and its binary mixtures with dimethyl sulfoxide, J. Mol. Liq., 225 (2017) 689-695.
[32] R.B. Leron, D.S.H. Wong, M.-H. Li, Densities of a deep eutectic solvent based on choline chloride and glycerol and its aqueous mixtures at elevated pressures, Fluid Phase Equilib., 335 (2012) 32-38.
[33] A.P. Abbott, D. Boothby, G. Capper, D.L. Davies, R.K. Rasheed, Deep eutectic solvents formed between choline chloride and carboxylic acids: Versatile alternatives to ionic liquids, J. Am. Chem. Soc., 126 (2004) 9142-9147.
[34] G. D. Lee, C. Z. Wang, E. Yoon, N. M. Hwang, D. Y. Kim and K. M. Ho, *Phys. Rev. Lett*., 2005, **95**, 205501.
[35] A. Hashimoto, K. Suenaga, A. Gloter, K. Urita and S. Iijima, *Nature*, 2004, **430**, 870–873.
[36] S. Grimme, J. Antony, S. Ehrlich, H. Krieg, A consistent and accurate ab initio parametrization of density functional dispersion correction (DFT-D) for the 94 elements H-Pu, Chem. Phys. 132 (2010) 154104.
[37] M. Shakourian-Fard, Z. Jamshidi, A. Bayat, G. Kamath, Meta-Hybrid Density Functional Theory Study of Adsorption of Imidazolium- and Ammonium-Based Ionic Liquids on Graphene Sheet, J. Phys. Chem. C. 119 (2015) 7095-7108.
[38] M. Shakourian-Fard, G. Kamath, The effect of defect types on the electronic and optical properties of graphene nanoflakes physisorbed by ionic liquids, Phys. Chem. Chem. Phys. 19 (2017) 4383-4395.
[39] M. Shakourian-Fard, G. Kamath, Z. Jamshidi, Trends in Physisorption of Ionic Liquids on Boron-Nitride Sheets, J. Phys. Chem. C. 118 (2014) 26003-26016.
[40] M. Shakourian-Fard, A. Bayat, G. Kamath, Effect of mono-vacant defects on the opto-electronic properties of ionic liquid functionalized hexagonal boron-nitride nanosheets, J. Mol. Liq. 249 (2018) 1172-1182.
[41] M. Shakourian-Fard, H.R. Ghenaatian, G. Kamath, S.M. Taimoory, Unraveling the effect of nitrogen doping on graphene nanoflakes and the adsorption properties of ionic liquids: A DFT study, J. Mol. Liq. 312 (2020) 113400.

[42] M. Shakourian-Fard, S. Maryamdokht Taimoory, V. Semeniuchenko, G. Kamath, J.F. Trant, The effect of ionic liquid adsorption on the electronic and optical properties of fluorographene nanosheets, J. Mol. Liq. 268 (2018) 206-214.
[43] E.S. Zarudnev, S.G. Stepanian, L. Adamowicz, V.S. Leontiev, V.A. Karachevtsev, Comparison of noncovalent interactions of zigzag and armchair carbon nanotubes with heterocyclic and aromatic compounds: Imidazole and benzene, imidazophenazines, and tetracene, Chem. Phys. 483-484 (2017) 68-77.
[44] M.J. Frisch, G.W. Trucks, H.B. Schlegel, G.E. Scuseria, M.A. Robb, J.R. Cheeseman, G. Scalmani, V. Barone, B. Mennucci, G.A. Petersson, H. Nakatsuji, M. Caricato, X. Li, H.P. Hratchian, A.F. Izmaylov, J. Bloino, G. Zheng, J.L. Sonnenberg, M. Hada, M. Ehara, K. Toyota, R. Fukuda, J. Hasegawa, M. Ishida, T. Nakajima, Y. Honda, O. Kitao, H. Nakai, T. Vreven, J.A. Montgomery Jr., J.E. Peralta, F. Ogliaro, M.J. Bearpark, J. Heyd, E.N. Brothers, K.N. Kudin, V.N. Staroverov, R. Kobayashi, J. Normand, K. Raghavachari, A.P. Rendell, J.C. Burant, S.S. Iyengar, J. Tomasi, M. Cossi, N. Rega, N.J. Millam, M. Klene, J.E. Knox, J.B. Cross, V. Bakken, C. Adamo, J. Jaramillo, R. Gomperts, R.E. Stratmann, O. Yazyev, A.J. Austin, R. Cammi, C. Pomelli, J.W. Ochterski, R.L. Martin, K. Morokuma, V.G. Zakrzewski, G.A. Voth, P. Salvador, J.J. Dannenberg, S. Dapprich, A.D. Daniels, Ö. Farkas, J.B. Foresman, J.V. Ortiz, J. Cioslowski, D.J. Fox, Gaussian 09, Gaussian, Inc, Wallingford, CT, USA, 2009.
[45] S.F. Boys, F. Bernardi, The calculation of small molecular interactions by the differences of separate total energies. Some procedures with reduced errors, Mol. Phys. 19 (1970) 553-566.
[46] C.M. Breneman, K.B. Wiberg, Determining atom-centered monopoles from molecular electrostatic potentials. The need for high sampling density in formamide conformational analysis, J. Comput. Chem. 11 (1990) 361-373.
[47] R.G. Parr, R.G. Pearson, Absolute hardness: companion parameter to absolute electronegativity, J. Am. Chem. Soc. 105 (1983) 7512-7516.
[48] E.R. Johnson, S. Keinan, P. Mori-Sánchez, J. Contreras-García, A.J. Cohen, W. Yang, Revealing Noncovalent Interactions, J. Am. Chem. Soc. 132 (2010) 6498-6506.
[49] K. Morokuma, Molecular Orbital Studies of Hydrogen Bonds. III. C=O···H–O Hydrogen Bond in H2CO···H2O and H2CO···2H2O, Chem. Phys. 55 (1971) 1236-1244.
[50] T. Ziegler, A. Rauk, On the calculation of bonding energies by the Hartree Fock Slater method, Theor. Chim. Acta. 46 (1977) 1-10.

[51] T. Lu, F. Chen, Multiwfn: A multifunctional wavefunction analyzer, J. Comput. Chem. 33 (2012) 580-592.
[52] W. Humphrey, A. Dalke, K. Schulten, VMD: Visual molecular dynamics, J. Mol. Graph. 14 (1996) 33-38.
[53] E.J. Baerends, T. Ziegler, J. Autschbach, D. Bashford, A. Bérces, F.M. Bickelhaupt, C. Bo, P. Boerrigter, L. Cavallo, D. Chong, ADF2013, Software for Chemistry & Materials, 2014.
[54] G. te Velde, F.M. Bickelhaupt, E.J. Baerends, C. Fonseca Guerra, S.J.A. van Gisbergen, J.G. Snijders, T. Ziegler, Chemistry with ADF, J. Comput. Chem. 22 (2001) 931-967.
[55] F.M. Bickelhaupt, E.J. Baerends, Reviews in Computational Chemistry, 2000, p. 1-86.
[56] A. Spreinat, M.M. Dohmen, J. Lüttgens, N. Herrmann, L.F. Klepzig, R. Nißler, S. Weber, F.A. Mann, J. Lauth, S. Kruss, Quantum Defects in Fluorescent Carbon Nanotubes for Sensing and Mechanistic Studies, J. Phys. Chem. C. 125 (2021) 18341-18351.
[57] A. Hendler-Neumark, G. Bisker, Fluorescent Single-Walled Carbon Nanotubes for Protein Detection, Sensors. 19 (2019) 5403.
[58] J.-H. Huang, Y.-J. Hong, Y.-T. Chang, P. Chang, T.-R. Yew, Carbon nanotubes for highly sensitive colorimetric immunoassay biosensor, J. Mater. Chem. B. 1 (2013) 5389-5392.
[59] S.M. Bachilo, M.S. Strano, C. Kittrell, R.H. Hauge, R.E. Smalley, R.B. Weisman, Structure-Assigned Optical Spectra of Single-Walled Carbon Nanotubes, Science. 298 (2002) 2361-2366.